Harmonic analysis and isotopic investigation for recharge area characterization of the Promise Spring (Aosta Valley, NW Italy)

Hydrogeology Journal
https://doi.org/10.1007/s10040-025-02923-1

REPORT

Harmonic analysis and isotopic investigation for recharge area characterization of the Promise Spring (Aosta Valley, NW Italy)

Martina Gizzi[1] · **Luca Biamino**[1]

Received: 8 November 2024 / Accepted: 5 June 2025

Abstract
The response of alpine aquifer systems to changing climatic conditions is dependent on the specific geographical and geological context. Consequently, understanding fluctuations in hydrogeological balances at the scale of spring catchments has become increasingly crucial for anticipating future scenarios related to water availability. This study focuses on Promise Spring in the Aosta Valley region (NW Italy) between October 2011 and July 2024 and employs innovative methodologies, including Fourier transform analysis, to characterize spring hydrograph signals and their relationships with atmospheric temperature, snow depth, and rainfall data. In addition, isotopic analyses of water samples were conducted to gain a better understanding of the origin of the water that feeds the spring. The analysis of the hydrodynamic behavior of the spring revealed a clear correlation between the environmental variables and their temporal variations. The main discharge peaks were associated with the completion of the snowmelt process between April and May, indicating that snowmelt was one of the primary water sources that fed the spring. Recent increases in discharge and the temporal shift of the recession curve minima toward the autumn and winter months are attributable to altered meteorological conditions that have modified snow accumulation regimes at higher altitudes in the catchment area. Isotopic analyses revealed that the Promise Spring exhibited an isotopic composition that is indicative of the absence of glacial paleowater contributions and implies a primarily meteoric origin derived from snowmelt and precipitation.

Keywords Groundwater recharge · Fourier analysis · Stable isotopes · Aosta Valley springs · Italy

Introduction

Mountain hydrology and hydrogeology in the European Alps have undergone significant changes over the last few decades due to climate change, land use changes, and altered water consumption patterns and policies. In particular, climate change has influenced the characteristics of droughts and floods, evapotranspiration, snow–rainfall ratios, and snow seasonality, and has resulted in new rainfall patterns associated with rising average air temperatures (Carroll et al. 2019; Crepaldi et al. 2015; de Palézieux and Loew 2019; Donnelly et al. 2017; Jódar et al. 2020; Kim and Villarini 2023; Mondani et al. 2022; Newlands et al. 2015; Riedel and Weber 2020; Xanke and Liesch 2022; Xanke et al. 2024). In addition, complementary decreases in precipitation have resulted in droughts, which have been responsible for reduced snow cover in winter and shorter snow seasons in spring (Wu et al. 2018; Wu et al. 2020). The response of the alpine environmental systems to the aforementioned conditions has resulted in a reduction in groundwater circulation due to decreased rainfall and snow thickness across the different hydrometeorological seasons (Dey et al. 2020; Mo et al. 2019; Szwed 2019). Consequently, gaining a deeper understanding of fluctuations in hydrological balances is increasingly important for predicting future scenarios related to water availability (Duratorre et al. 2020; Wang et al. 2023; Zuecco et al. 2019).

Over the last few decades, several different authors have analyzed meteorological data in an attempt to describe the relationship between changes in weather conditions and water availability in the Aosta Valley region. Gizzi et al. (2022) reported that not all of the springs investigated in the Aosta Valley springs appear to be affected by reductions in solid and liquid precipitation inputs, despite precipitation

✉ Luca Biamino
luca.biamino@polito.it

[1] Department of Environment, Land and Infrastructure Engineering (DIATI), Politecnico Di Torino, C.So Duca Degli Abruzzi 24, 10129 Turin, Italy

Published online: 07 July 2025

data from the selected meteorological stations revealing an overall decreasing trend in annual rainfall (mm) and a slight increase in rainfall intensity (mm/day) due to the reduction in rainfall events (i.e., number of rainy days). Furthermore, Orusa et al. (2021) explored the effects of short-term climate change effects on phenological metrics and the evapotranspiration of the rangelands and broad-leaved forests of the Aosta Valley using remotely sensed data; they found that, like many other alpine regions, the Aosta Valley is currently suffering from significant temperature increases as a result of climate change, which has driven significant changes in the growing seasons of the rangelands.

In the context of the Italian Alps, increases in air temperature are strongly influenced by altitude. Indeed, higher altitudes were found to be more sensitive to rising temperatures, leading to the reduced persistence of snowpacks. Consequently, these regions are among the most severely and rapidly affected ecosystems due to being susceptible to changes in temperature and precipitation patterns at all scales (Stöckli and Vidale 2004).

Satellite observations recorded by Cabina di Regia dei Ghiacciai Valdostani (2022) revealed a 24 km^2 reduction in glacial surface area in the Aosta Valley since 1999. Additionally, the temporary snow resource, which plays a critical role in feeding water bodies, has decreased by 23% over the last 20 years. Indeed, snow and ice are the main controls on the hydrological cycle, and their variations can affect the entire geosystem, including rocks, soils, vegetation, and river discharges and especially seasonal runoff (Colucci and Guglielmin 2019; Corte et al. 2024; Thibert et al. 2018; Vergnano et al. 2023; Zemp et al. 2015). In particular, the melting of glaciers and permafrost is currently compensating for water scarcity by providing relevant volumes of water every year.

Determining the contribution of permanent cryosphere melting in the context of altered spring discharge volumes is essential to gain a medium-term understanding of water balance alterations in alpine regions. Numerous methodologies have been developed over the last few decades to obtain hydrogeological information about recharging systems in mountain springs. Hydrographs represent the final output from the various processes that govern the transformation of precipitation and other water inputs in the drainage area. Consequently, spring recession curves were analyzed to determine the hydrological properties of aquifers as well as to quantitatively estimate the evolution of water resources over time (Cerino Abdin 2021; Kresic and Bonacci 2010; Lo Russo et al. 2014, 2021). In this study, Promise Spring, located in the Aosta Valley (NW Italy), was selected as a case study. This site is well-suited to the context of climate change impacts on water resources, as recent studies have reported increases in both maximum and minimum discharge values over multi-year time series data (Gizzi et al. 2022). This behavior cannot be immediately explained within the framework of changing climate conditions and requires innovative methodologies to obtain a more detailed characterization of the inputs that feed the aquifer. Here, a Fourier transform analysis of the spring hydrograph signal was used to characterize the main signal harmonics and relate them to other environmental variables (Balugani and Antonellini 2011; Neto et al. 2016; Rahi and Halihan 2013; Solórzano-Rivas et al. 2021). Specifically, the spring hydrograph, rainfall, snow depth, and temperature signals were decomposed; their spectrograms were analyzed to identify the physical relationships between these parameters. This approach was previously employed by some authors to understand changes in groundwater response due to cryosphere melting (Magnusson et al. 2014; Pasquini et al. 2008; Xie et al. 2006): however, the application of Fourier transform analysis to a time series of physical variables in order to identify the long-term harmonic components of these variables has been relatively limited.

The results obtained were further combined with isotopic analyses performed on water samples according to the V-SMOW standard. Measurements of oxygen-18 ($\delta^{18}O$) and deuterium ($\delta^{2}H$) have proven to be crucial for understanding flow paths in both surface water and groundwater, highlighting their broad applicability (Chizhova et al. 2022; Craig 1961a, b; Santillán-Quiroga et al. 2023; Thakur et al. 2020; Yu et al. 2021). In addition, the altitude of rainfall or snowfall deposition was assessed using empirical relationships available in the literature (Bortolami et al. 1979; Giustini et al. 2016; Mazor 2004; Novel et al. 1995). The synthesis of results from these two independent analysis techniques has provided further insights into the nature and origin of the water inputs that feed Promise Spring. Consequently, the results presented in this research extend beyond simple discharge trend evaluations and instead offer a deeper understanding of the spring's variability in both short- and long-term scenarios.

Materials and methods

Study area

The Aosta Valley region is geographically located in the northwestern part of the Italian Peninsula. It is characterized by a typical alpine climate, with cold winters and cool summers. Monthly rainfall peaks in spring and autumn, with the lowest values recorded in summer and winter. The highest mean monthly precipitation is approximately 140 mm, while the minimum mean precipitation is approximately 30 mm (Mercalli et al. 2003).

Approximately 30% of the Aosta Valley region is 2500 m above sea level (a.s.l.), with glaciers covering around 4.8%

of the region (representing a glacial surface area of approximately 120 km^2) (Cabina di Regia dei Ghiacciai Valdostani 2022). The Rutor Glacier is one of the largest glaciers in the region: its altitude ranges from around 2550 m a.s.l., where its ice body forms two main tongues, to around 3400 m a.s.l., near Testa del Rutor (max. 3486 m a.s.l.) (Corte et al. 2024; Vergnano et al. 2023). The Rutor Glacier faces northwest and has a specific conformation that minimizes the risk of ice block failures and snow avalanches. Meltwater from ice and snow flows into the main drainage channel, known as the Rutor Torrent, which passes through the municipality of La Thuile and flows toward the Dora Baltea River (Fig. 1).

Promise Spring is located downstream of the Rutor Glacier at an elevation of 1580 m a.s.l., near the municipality of La Thuile, and lies on the right bank of the Rutor Torrent (Gizzi et al. 2022). The aquifer complex that feeds Promise Spring is embedded within layers of conglomerates and metapelites that alternate with schists and micaceous sandstones. These rock layers have dip angles of 35–39° with a dip direction of 105–115°N (E–SE). The spring's outflow emerges through the drainage gallery system of an abandoned underground mines (Morgex-La Thuile Complex). Groundwater also flows through a complex network of fractures generated by rock-laying surfaces and a regional vertical fault that runs beneath the glacier (Figs. 2 and 3). In addition, a vertical fault crosses the Rutor Torrent and extends uphill toward the spring. This fault creates a hydrogeological boundary that confines the aquifer between the Rutor Torrent and the fault. The Promise Spring is situated in a topographic saddle on the slope, where the piezometric level reaches the drainage gallery that channels groundwater towards the surface (Gizzi et al. 2022). The average temperature of the spring water is about 10 °C; the spring water is not derived from rapid infiltration and instead undergoes modest underground groundwater circulation before reaching the outlet.

Figure 1 shows the location of the Villaret weather station (1488 m a.s.l.). This station collects data on air temperature, snow depth, and rainfall, and is close to also where the Rutor Torrent is sampled (2130 m a.s.l.); the sampling point is located immediately above the Rutor Falls, where samples were collected for isotopic analysis.

Time series analysis

The cause-and-effect relationships in the temporal evolution of the spring's hydrogeological system were assessed through the analysis of several variables between October 2011 and July 2024. The mean daily values of the air temperature (T_{air}), snow depth (SD), and rainfall (RF) were obtained from the Villaret weather station (managed by the Aosta Valley Autonomous Region Environmental Protection Agency) over this period. Precipitation was measured using a tipping-bucket rain gauge, which lacks a heating system and was thus unable to precisely differentiate between rain and snowfall. The discharge (Q) was monitored at Promise Spring using multi-probes (Corr-Tek Idrometria). The hydrometric level was measured with an hourly frequency and a mm-level resolution. These measurements were converted into discharge values using Eq. (1).

$$Q = 0.385 \cdot h_0^{1.5} b \sqrt{2g} \tag{1}$$

This equation was applied to a Bélanger rectangular weir, where h_0 represents the hydraulic head and b represents the width.

Hydrographs represent the result of several processes that mediate the transformation of precipitation and other water inputs in the drainage area into a single output. Hydrographs are constructed based on discharge values measured over a hydrogeological year, and their shape is dependent on the size of the drainage area and the intensity of precipitation (Kresic and Bonacci 2010).

The Promise Spring hydrograph represents the main outflow of the aforementioned hydrogeological system and offers a series of observations associated with the characteristics and behavior of the aquifer. Consequently, the evolution of the water resources within the rock mass can be quantitatively described in terms of annual average variations using a regression line equation (Cerino Abdin 2021).

Snowmelt evaluation

The hydrological input was obtained by estimating the volume of liquid water that recharges the aquifer. To achieve this, the contribution of snowpack melting must be converted into an equivalent volume of liquid water released into the environment based on the relevant meteorological conditions. The snow water equivalent (SWE) index (2) accounts for factors such as snowpack compaction and metamorphism, both of which increase the density of fresh snow, thereby providing an equivalent measurement in terms of liquid water (DeWalle and Rango 2008). This study assumed an average density of 100 kg/m^3; however, it should be noted that densities during melting can sometimes reach values of 400–600 kg/m^3. Indeed, the ablation process is primarily influenced by air temperatures that exceed 0 °C; other factors include solar radiation, relative humidity, and air pressure (Longoni et al. 2022). The daily SWE for the Villaret weather station was reconstructed by converting solid precipitation inputs into water equivalents as winter transitions into spring.

$$\mathrm{SWE} = \frac{\text{Snow density}\left(\frac{\mathrm{kg}}{\mathrm{m}^3}\right)}{\text{Water density}\left(\frac{\mathrm{kg}}{\mathrm{m}^3}\right)} \cdot \text{Snow depth (SD)(cm)} = 0.1 \cdot \mathrm{SD\ (cm)} \tag{2}$$

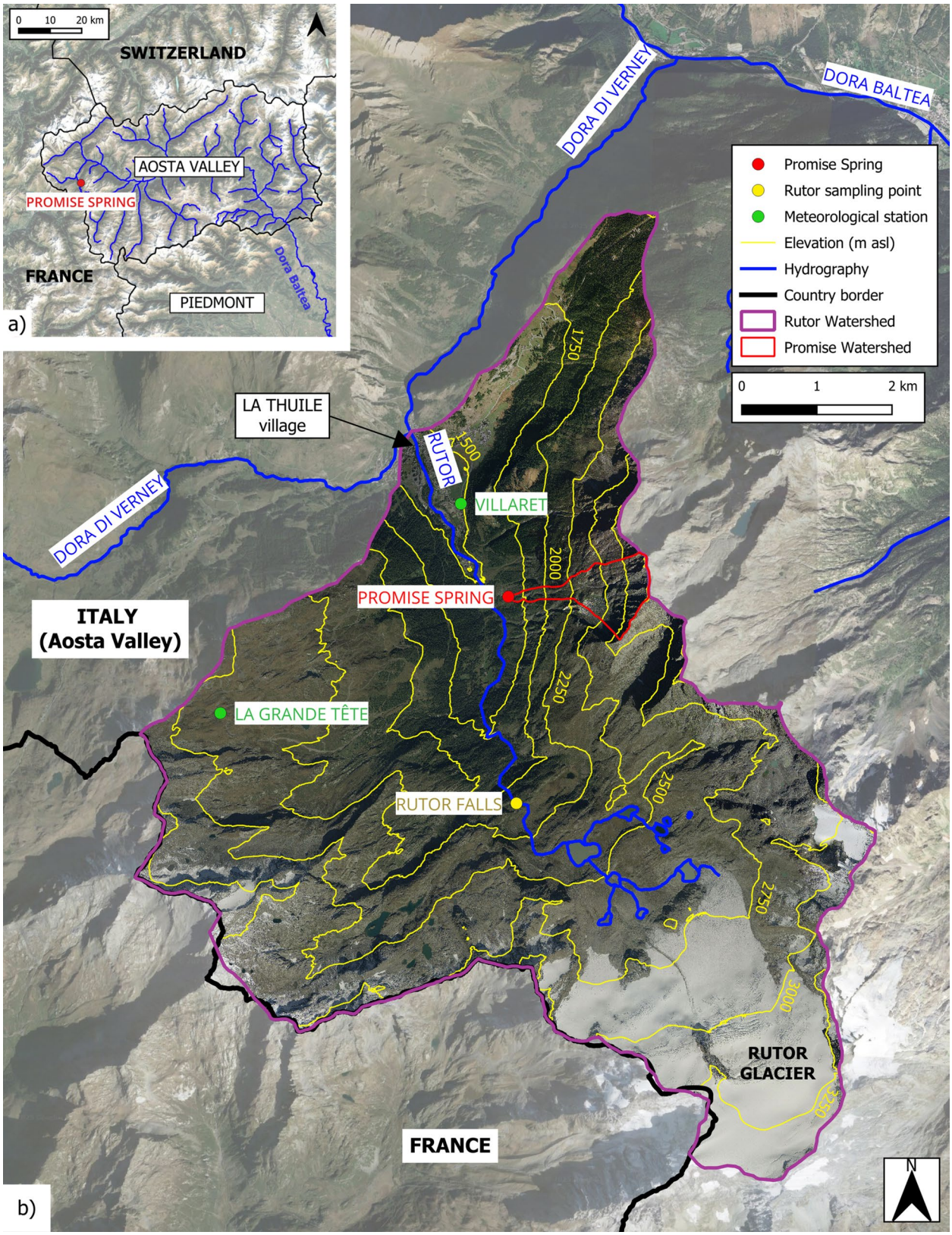

Fig. 1 Overview of the study area. **a** Location of Promise Spring in the Aosta Valley region. **b** Detailed map of the Rutor Torrent watershed, including the location of the Villaret (La Thuile municipality) weather station, the Promise Spring catchment area, and the Rutor Falls sampling point. Basemap: Google satellite web map service QuickMapServices plugin; orthophoto Aosta Valley Autonomous Region Geoportale (**b**). Edited in QGIS v. 3.34.11 (**a**, **b**)

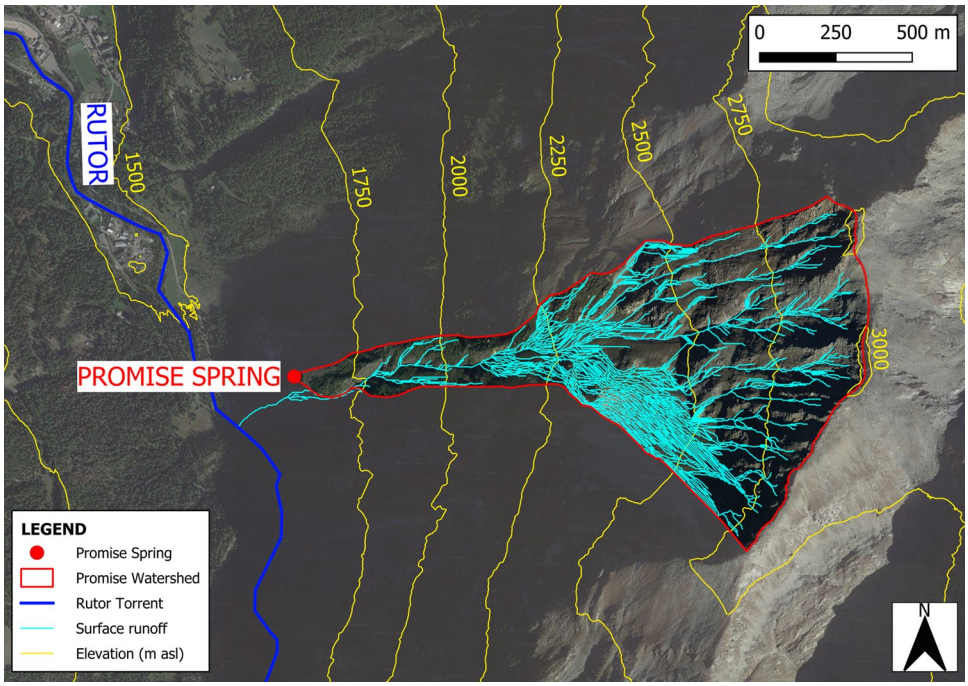

Fig. 2 The Promise Spring watershed, as indicated by the *red line*. Surface runoff was reconstructed using SAGA GIS software v. 9.5.1 from the DTM model available on Aosta Valley Autonomous Region Geoportale. Basemap: orthophoto from the Aosta Valley Autonomous Region Geoportale

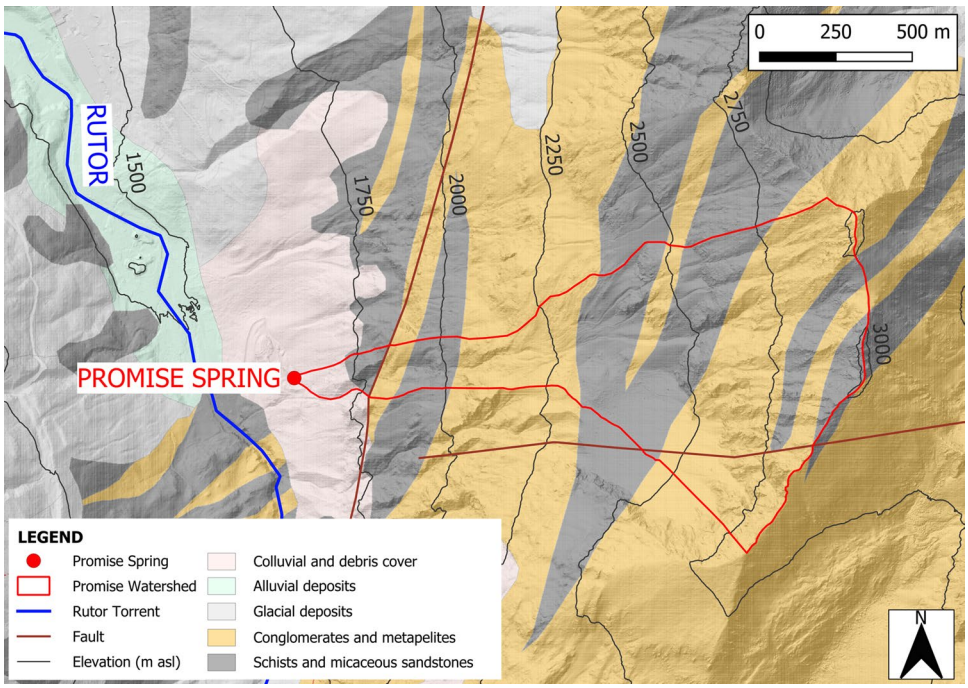

Fig. 3 Geological context of the Promise watershed. It should be noted that the selected spring drains only a portion of the surface runoff due to fractures in the rock mass as well as several stratigraphical discontinuities that affect the outcropping formations. Surface runoff that is not intercepted flows directly into the Rutor Torrent without feeding the aquifer. Basemap: Geological Map scale 1:100000 available on Aosta Valley Autonomous Region Geoportale

Fourier transform and harmonic analysis

The Fourier transform is a fundamental technique for analyzing the frequency content of signals. It is based on Fourier's Theorem, which states that any periodic function $x(t)$ with a period τ (or analogously a fundamental frequency $\Omega_0 = 2\pi/\tau$) can be decomposed into an infinite series of sine and cosine functions according to Eq. (3). Coefficients a_0, b_0 and b_k are given by Eqs. (4), (5), and (6) respectively (Leis 2011).

$$x(t) = a_0 + \sum_{k=1}^{\infty} (a_k \cos k\Omega_0 t + b_k \sin k\Omega_0 t) \tag{3}$$

$$a_0 = \int_0^{\tau} x(t)\mathrm{d}t \tag{4}$$

$$a_k = \frac{2}{\tau}\int_0^{\tau} x(t)\cos k\Omega_0 t\,\mathrm{d}t \tag{5}$$

$$b_k = \frac{2}{\tau}\int_0^{\tau} x(t)\sin k\Omega_0 t\,\mathrm{d}t \tag{6}$$

The Fourier transform does not strictly require the signal to have a periodic structure for processing. Specifically, the discrete-time Fourier transform requires a signal $x(t)$ that is sampled at time instants $t = nT$, where n is an integer and T is the temporal distance recorded between two consecutive samples. In contrast, the continuous Fourier transform (7) is based on the conversion from the continuous time domain into its frequency counterpart $X(\Omega)$ (where Ω is the true frequency in radians per second). This allows the statement to be rewritten as Eq. (8) and introduces the frequency $\omega = \Omega T$ (expressed in radians/sample) (Leis 2011).

$$X(\Omega) = \int_{-\infty}^{\infty} x(t)\mathrm{e}^{-j\Omega t}\mathrm{d}t \tag{7}$$

$$X(\Omega) = \sum_{n=-\infty}^{+\infty} x(n)\mathrm{e}^{-jn\omega} \tag{8}$$

The final step is represented by the discrete Fourier transform (DFT) (9), which converts a sampled time domain into a sampled frequency domain. The frequency of the k^{th} sinusoid ω_k is expressed as $(2\pi k)/N$, where N is the number of acquired samples (Leis 2011). Since the computational cost of the DFT is relatively high, the fast Fourier transform (FFT) algorithm was developed and is currently preferable when calculating the transform using numerical software (Brigham and Morrow 1967).

$$X(k) = \sum_{n=0}^{N-1} x(n)\mathrm{e}^{-jn\omega_k} \tag{9}$$

The data were resampled to mean daily values (i.e., a sampling frequency of one measurement per day) to eliminate the occurrence of small hourly probe spikes that could affect the quality of the signal. Furthermore, a threshold frequency corresponding to 1 year ($1/365 \approx 0.00274$) was implemented in the amplitude spectrogram: lower frequency values should describe long-term effects, while the highest frequency values should define the spring's behavior over a single hydrogeological year.

The time series of the examined variables was reconstructed using harmonic series analysis. In this technique, the input is the frequency spectrogram obtained with the FFT. Indeed, the mathematical expression of the Fourier series (Eq. 3) (Schmidt et al. 2008) should be able to distinguish and allow for the reconstruction of both the long- and short-term components in the original signals through a discrete summation of the harmonics.

Isotopic analyses

Water is characterized by the presence of several isotopic compounds, with the two most relevant isotopes being oxygen-18 ($\delta^{18}O$) and deuterium ($\delta^{2}H$). The isotopic composition of the samples was determined by mass spectrometry and expressed in per mil deviations from the Vienna Standard Mean Ocean Water (V-SMOW) (Mazor 2004). Isotopic analyses were performed at the ISO4 Laboratory (Department of Earth Sciences, University of Turin) using wavelength-scanned cavity ring-down spectroscopy (WS-CRDS). Two samples were collected on 8 July 2024: the former was taken from Promise Spring, while the latter was collected from the Rutor Falls, which are fed by glacial meltwater (see Fig. 1). The obtained results were compared with local meteoric water lines (LMWL), which serve as a useful tool for tracing the origin and movements of groundwater in specific geological contexts. Indeed, in cases when the isotopic values are aligned with some lines in the $\delta^{2}H$–$\delta^{18}O$ diagram, the relevance of secondary processes (e.g., evaporation prior to infiltration in the rock fractures) can be considered negligible, reflecting the composition of precipitation (Mazor 2004). Equations (10)–(14) were utilized for this purpose (Table 1).

The isotopic composition of groundwater can also be associated with other physical effects, such as altitudinal effects: as clouds ascend, the residual precipitation becomes isotopically lighter (Leontiadis et al. 1983; Mazor 2004; Payne and Yurtsever 1974). An altitudinal gradient for the northwestern

Table 1 Local meteoric water lines (LMWLs) examined using the isotopic values from the Promise Spring and Rutor Falls sites

LMWL	Formula	Equation number	Citation
Global meteoric line	$\delta^{2}H = 8 \cdot \delta^{18}O + 10$	(10)	(Craig 1961a)
Northern hemisphere, continental	$\delta^{2}H = (8.1 \pm 1)\delta^{18}O + (11 \pm 1)$	(11)	(Dansgaard 1964)
Mediterranean or Middle East	$\delta^{2}H = 8 \cdot \delta^{18}O + 22$	(12)	(Gat 1971)
Maritime Alps (April 1976)	$\delta^{2}H = (8.0 \pm 0.1)\delta^{18}O + (12.1 \pm 1.3)$	(13)	(Bortolami et al. 1979)
Maritime Alps (October 1976)	$\delta^{2}H = (7.9 \pm 0.2)\delta^{18}O + (13.4 \pm 2.6)$	(14)	(Bortolami et al. 1979)

sector of the Aosta Valley was estimated using Eq. (15) based on $\delta^{18}O$ content (Giustini et al. 2016; Novel et al. 1995). Bortolami et al. (1979) used a different approach to develop an analytical model that estimated the recharge altitude h from isotopic hydrology in the Corsaglia Valley basin (Maritime Alps). Both of these equations map the $\delta^{18}O$ content to elevation and were developed in April 1976 (16) and October 1976 (17), respectively. Their combination yields an average annual gradient expressed by Eq. (18); a further relation for the deuterium content is provided by Eq. (19). Both isotopic gradient and empirical equation methods were tested in this study, and their reliability in the context of the selected site is explored in the discussion section.

$$\frac{\delta^{18}O}{100\ \text{m}} = -0.23‰ \tag{15}$$

$$\delta^{18}O\,‰ = -(3.10 \pm 0.14) \cdot 10^{-3} \cdot h - (8.24 \pm 0.18) \tag{16}$$

$$\delta^{18}O\,‰ = -(3.17 \pm 0.08) \cdot 10^{-3} \cdot h - (7.85 \pm 0.14) \tag{17}$$

$$\delta^{18}O\,‰ = -(3.12 \pm 0.10) \cdot 10^{-3} \cdot h - (8.03 \pm 0.13) \tag{18}$$

$$\delta^{2}H\,‰ = -(24.9 \pm 0.8) \cdot 10^{-3} \cdot h - (51.1 \pm 0.6) \tag{19}$$

Results

Times series data for snow depth (SD), rainfall (RF), air temperature (T_{air}), and discharge (Q) in Promise Spring are illustrated in Fig. 4. Snow accumulation has decreased considerably since 2018, with depths no longer exceeding 100 cm and currently stabilizing below 50 cm, with complete melt occurring by the end of April. The SWE index was evaluated by assuming a snow density of 100 kg/m^3 (Eq. 2); these values are presented on the y-axis of Fig. 4a

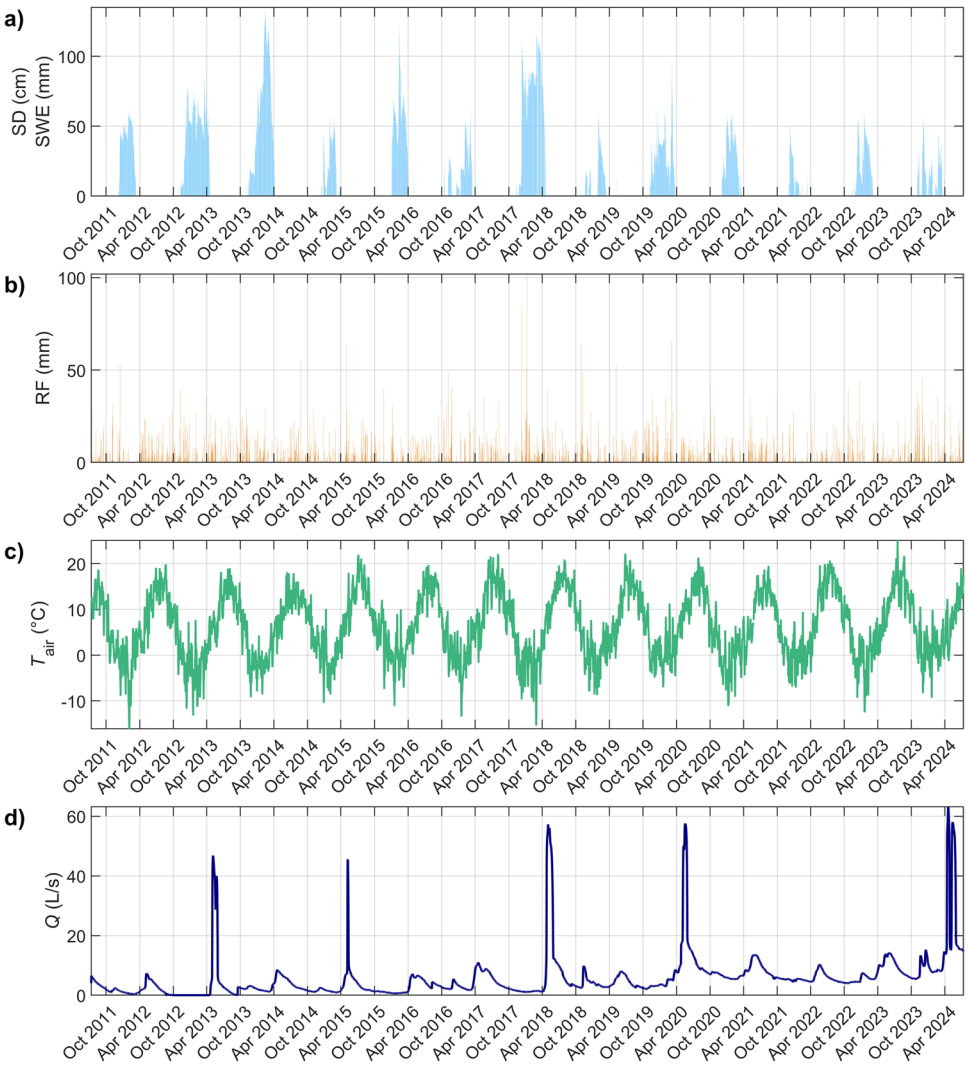

Fig. 4 Time series of **a** daily snow depth (SD), **b** daily rainfall (RF), and **c** daily mean air temperature (T_{air}) data from Villaret weather station. **d** Daily average discharge values measured in Promise Spring

Table 2 Maximum and minimum discharge values measured at Promise Spring over the last few hydrogeological years

Hydrogeological year	Annual minimum values		Annual maximum values	
	Date	Discharge (l/s)	Date	Discharge (l/s)
2013–2014	Mar 7, 2014	1.15	Apr 20, 2014	8.57
2014–2015	Mar 9, 2015	0.89	May 9, 2015	45.54
2015–2016	Feb 1, 2016	0.59	Apr 25, 2016	7.15
2016–2017	Mar 1, 2017	1.67	Apr 19, 2017	10.97
2017–2018	Jan 23, 2018	1.12	May 3, 2018	57.30
2018–2019	Mar 21, 2019	2.65	Jun 7, 2019	8.00
2019–2020	Oct 19, 2019	2.06	May 19, 2020	57.60
2020–2021	Feb 19, 2021	5.37	Jun 4, 2021	13.56
2021–2022	Dec 25, 2021	4.30	May 18, 2022	10.30
2022–2023	Dec 22, 2022	4.26	Jun 1, 2023	14.25
2023–2024	Oct 29, 2023	5.41	Apr 19, 2024	63.20

alongside snow depth. The reduction in snowpack appears to have altered the aquifer inflow pattern, resulting in higher volumes of liquid precipitation that directly infiltrate into the fractured supply network of the aquifer (Fig. 4b). The mean daily air temperatures (Fig. 4c) fluctuate between a minimum of − 10 °C in January and a maximum of 20 °C in July.

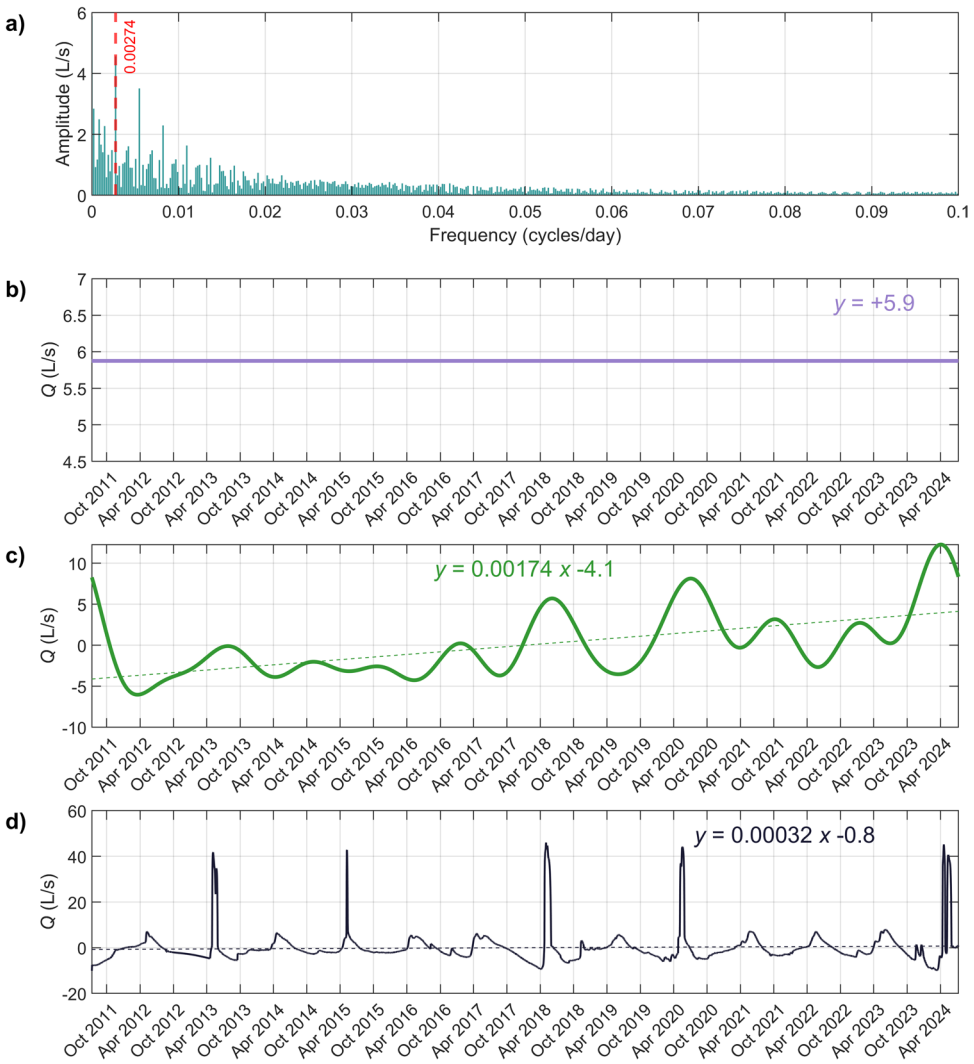

Fig. 5 Fourier transform and harmonic series analysis performed on daily mean discharge data from Promise Spring. **a** Amplitude–frequency spectrogram; **b** Fundamental frequency indicating the mean value of the signal; **c** Long-term component of the signal (corresponding to frequencies lower than 0.027) and its trend line; **d** Short-term component of the signal (corresponding to frequencies greater than 0.027) and its trend line

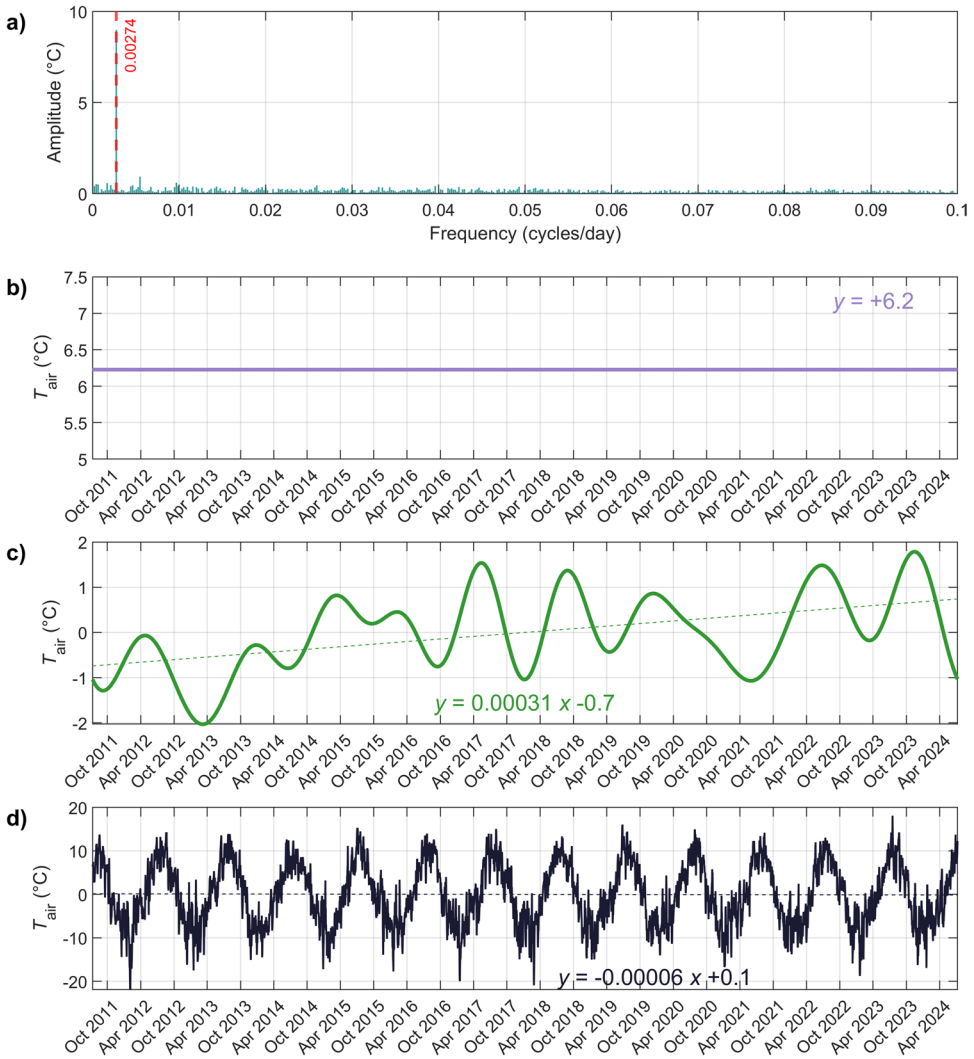

Fig. 6 Fourier transform and harmonic series analysis performed on daily mean air temperature data from the Villaret weather station. **a** Amplitude–frequency spectrogram; **b** Fundamental frequency indicating the mean value of the signal; **c** Long-term component of the signal (corresponding to frequencies lower than 0.027) and its trend line; **d** Short-term component of the signal (corresponding to frequencies greater than 0.027) and its trend line

Finally, Fig. 4d shows that significant flood peaks regularly occur around late April and early May. The minimum and maximum flow values over a single hydrogeological year (i.e., between October 1 and September 30) are summarized in Table 2. Both values have increased noticeably in recent years, with the minimum flows now occurring in late autumn rather than the final weeks of winter.

Figure 5 presents the analysis of the discharge values using FFT and reconstructed through the Fourier harmonic series described in Eq. (3): the resolution of the *x*-axis of the spectrogram in Fig. 5a is limited to a maximum frequency of 0.1, although in reality, it extends to the sampling frequency of one sample per day. The mean discharge value at the fundamental frequency is 5.87 l/s (Fig. 5b), while the long-term components exhibit an increasing trend that raises the discharge value to as high as 10 l/s (Fig. 5c). However, the main contributors to the flood peaks are short-term effects that can exceed 40 l/s: these trend lines remain almost constant across the entirety of the temporal dataset (Fig. 5d). Similar results were observed in the air temperatures recorded at the Villaret weather station (Fig. 6). In this case, however, the spectrogram clearly shows a single 0.00274 frequency peak (Fig. 6a). The mean temperature of 6.2 °C (Fig. 6b) was accompanied by an increasing trend in the long-term component that contributed nearly 2 °C (Fig. 6c), while the short-term component exhibited a consistent cyclic pattern over a 1-year period (Fig. 6d). The snow depth spectrogram exhibited two relevant peaks (Fig. 7a); the first peak corresponds to the standard 0.00274 value while the second peak exhibited a six-month periodicity (0.00548). Although a fundamental frequency of 11.7 cm was detected (Fig. 7b), the decreasing trend in the long-term component (Fig. 7c) was more relevant relative to the consistent short-term component (Fig. 7d). Finally, the rainfall spectrogram did not exhibit any prominent frequencies (Fig. 8a), other than a mean value of 2.3 mm (Fig. 8b). This observation was

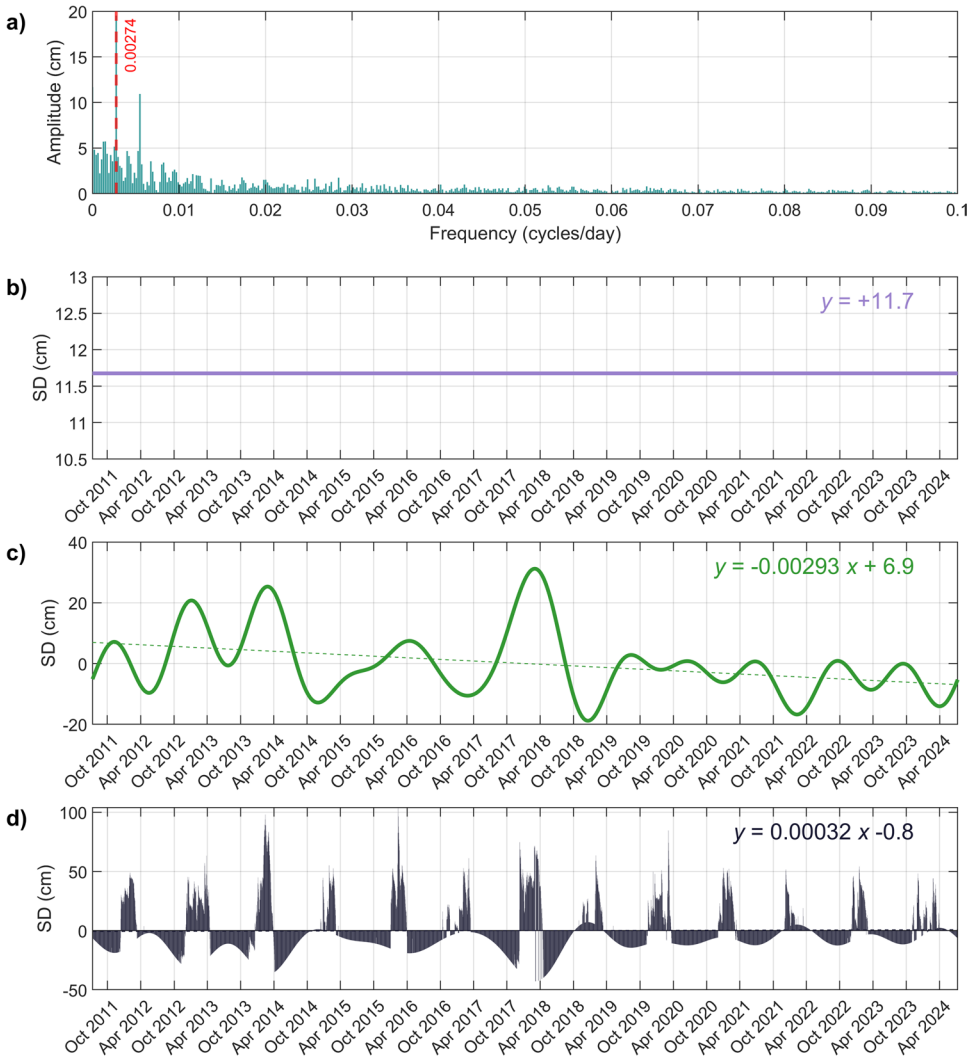

Fig. 7 Fourier transform and harmonic series analysis performed on daily snow depth data obtained from the Villaret weather station. **a** Amplitude–frequency spectrogram; **b** Fundamental frequency indicating the mean value of the signal; **c** Long-term component of the signal (corresponding to frequencies lower than 0.027) and its trend line; **d** Short-term component of the signal (corresponding to frequencies greater than 0.027) and its trend line

validated by Fig. 8c and d, in which the trend lines did not provide any information about relevant temporal variations in rainfall events.

Results of isotopic analysis performed on samples from Promise Spring and Rutor Falls are reported in Table 3. These values were compared to the LMWL to assess the influence of secondary processes on rainfall infiltration into the rock mass (Fig. 9 and Table 4). The $\delta^{18}O$ content also allows for the identification of the difference in altitude in the recharge areas of the two sites (Eq. 15), which was found to be 465 m. The estimated recharge altitudes are listed in Table 5; these were calculated by inverting Eqs. (16)–(19).

Discussion

The time series spring discharge data reported in Fig. 4 can be used to obtain useful information about the hydrodynamic behavior of Promise Spring and the evolution of its environmental variables, such as snow depth, rainfall, and air temperature. The main peaks in the spring discharge are attributable to the transfer of pressure induced by snowmelt: this phenomenon extends until the completion of this process between April and May, consistent with the results presented in Gizzi et al. (2022). In contrast, there was a clear correlation between rainfall and discharge volumes in autumn with a temporal lag of six hours; this was due to the liquid input rapidly recharging the aquifer without generating a prolonged pressure wave (Gizzi et al. 2023). Furthermore, starting from the 2018–2019 hydrological year, there was a clear increase in the discharge associated with the minimum recession values, in some cases exhibiting values that were considerably greater than 1 l/s (see Table 2). This was accompanied by a temporal shift toward the autumn and winter months. This appears to be a consequence of changes in meteorological conditions resulting in modified snow accumulation patterns at higher altitudes within the Promise basin.

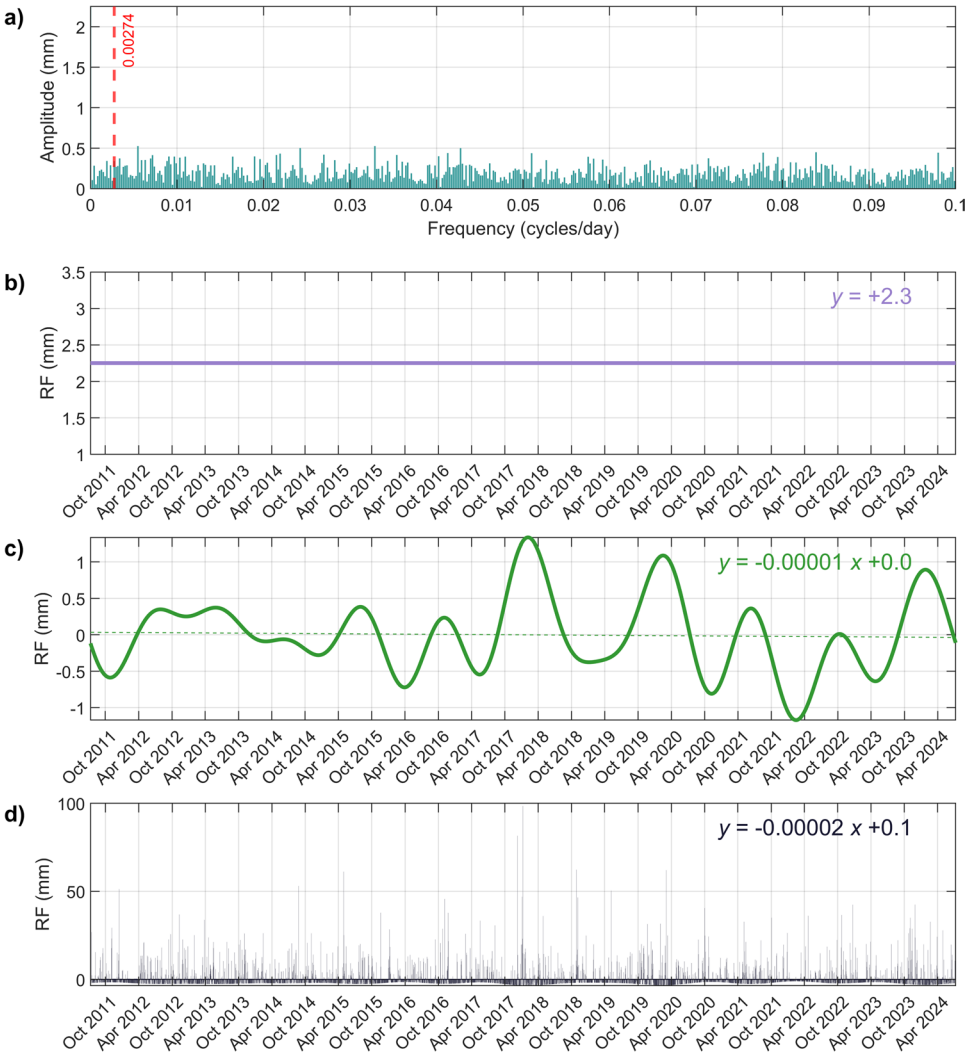

Fig. 8 Fourier transform and harmonic series analysis performed on daily rainfall data from the Villaret weather station. **a** Amplitude–frequency spectrogram; **b** Fundamental frequency indicating the mean value of the signal; **c** Long-term component of the signal (corresponding to frequencies lower than 0.027) and its trend line; **d** Short-term component of the signal (corresponding to frequencies greater than 0.027) and its trend line

The results of the harmonic analyses support the conclusions presented in the previous paragraph: the long-term components reconstructed from the amplitude spectrogram in Fig. 7c illustrate a decline in snow depth values recorded by the nivometer placed at the Villaret weather station. Simultaneously, the increasing trend in the long-term component of the atmospheric temperature (Fig. 6c) hindered snowfall in the Promise watershed. This resulted in an additional supply of liquid water to the fractured network of the Promise aquifer in October and November. The harmonic analysis of the rainfall data revealed additional insights (Fig. 8): as previously described in (Gizzi et al. 2022), unlike the increasing trends observed in the minimum air temperature and spring discharge values, there were no significant changes in precipitation trends (Fig. 8c). Indeed, the change in rainfall conditions had a relatively small effect on the hydrodynamic alterations at the Promise site. This is because the moderating factor is closely related to snowfall accumulation (which is dependent on air temperature) rather than the volume of liquid precipitation. It should be noted, however, that the intensity and temporal distribution varies greatly in this region.

Table 3 Isotopic composition of the samples collected from Promise Spring and Rutor Falls

Sample	$\delta^{18}O$ (‰)	Uncertainty $\delta^{18}O$ (‰)	$\delta^{2}H$ (‰)	Uncertainty $\delta^{2}H$ (‰)
Promise Spring 1580 m a.s.l	−13.44	±0.2	−96.17	±1
Rutor Falls 2130 m a.s.l	−14.51	±0.2	−100.83	±1

An isotopic analysis of the Rutor Falls samples links its waters back to its namesake glacier. This conclusion is supported by the general assumption that the Rutor Torrent is directly fed by glacial meltwater; however, further support can be found in research conducted in the Mont Blanc area (Novel et al. 1995), where the isotopic content of glacier samples shows a similar average $\delta^{18}O$ value of – 14.62 ‰ relative to the V-SMOW standard. In contrast, the Promise

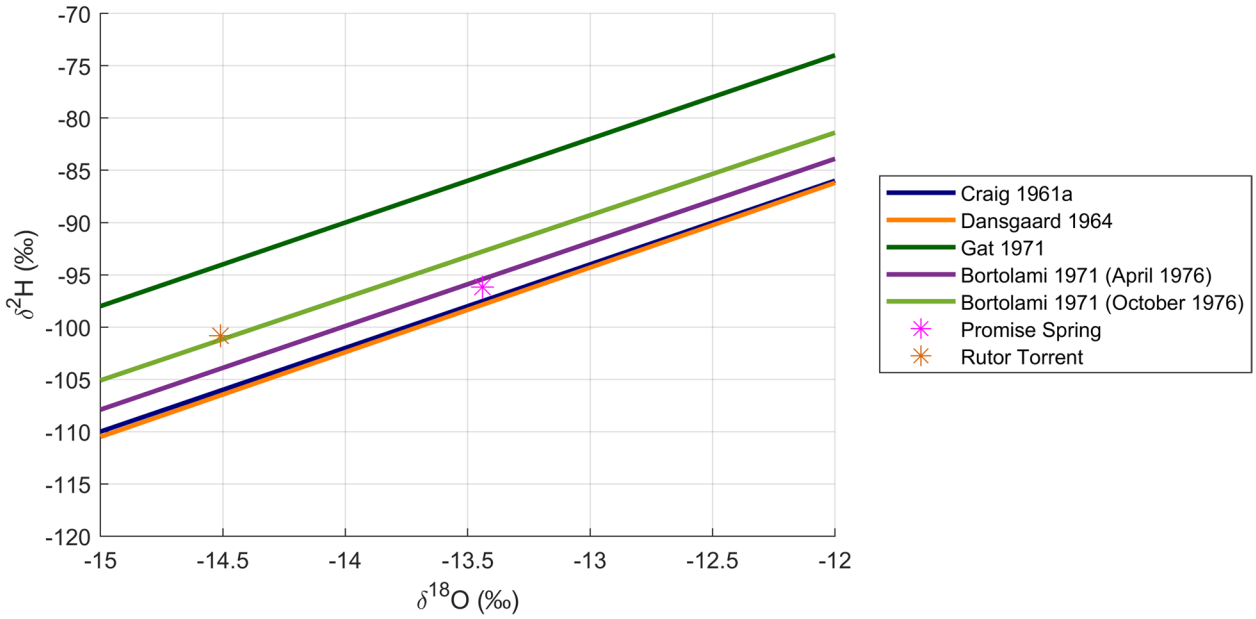

Fig. 9 Comparison between the local meteoric water lines (Mazor 2004) and the isotopic content in samples collected from Promise Spring and Rutor Falls

Table 4 Euclidean norm of the measured isotopic composition with respect to various local meteorological water lines (LMWLs)

Sample	Global meteoric line	Northern hemisphere continental	Mediterranean or Middle East	Maritime Alps (April 1976)	Maritime Alps (October 1976)
Promise Spring	0.1674 ‰	0.2076 ‰	1.3210 ‰	0.0930 ‰	0.4262 ‰
Rutor Torrent	0.6512 ‰	0.6985 ‰	0.8372 ‰	0.3907 ‰	0.0501 ‰

Spring samples were characterized by a higher isotopic content, indicating the absence of glacial inputs into the spring's feeding basin and a closer connection between the $\delta^{18}O$ and $\delta^{2}H$ content and the LMWL defined in the Maritime Alps in April 1976 (Bortolami et al. 1979) (Fig. 9). Indeed, the outflow of Promise Spring likely originates from snowmelt or rainfall. This mechanism can be considered analogous to that of the Corsaglia Valley, where no glacial masses are present within the watershed. Furthermore, the similarity in isotopic content between Promise Spring and precipitation confirms the absence of secondary processes that would alter the nature and origin of its waters. Conversely, there were no correlations between the isotopic content of the Rutor Falls sample and the October Meteoric Line defined by Bortolami et al. (1979) (Fig. 9) due to its glacial origin.

The altitude of the recharge areas was estimated using Eqs. (16)–(19). These values fall within the defined catchment area of the Promise Spring but are not consistent with the actual altitude of existing snow deposits. A more reliable result was obtained using the regional isotopic gradient (Eq. 15): by approximating the recharge area of the fractured Promise aquifer to be between 2500 and 3000 m a.s.l., the 465-m altitude difference obtained from this analysis supports the hypothesis that the waters feeding the Rutor Falls originate from the namesake glacier.

Table 5 Estimated altitude of the recharge areas for Promise Spring and the Rutor Torrent according to Eqs. (16)–(19)

Sample	Equation (15)	Equation (16)	Equation (17)	Equation (18)	Equation (19)
Promise Spring recharge altitude (m)	-	1677	1763	1734	1810
Rutor Torrent recharge altitude (m)	-	2022	2101	2077	1997
Elevation difference (m)	465	345	338	343	187

Conclusions

The response of alpine aquifer systems to changing climatic conditions is dependent on the specific geographical and geological context of the system. Consequently, understanding fluctuations in hydrogeological balances at the scale of spring catchments has become increasingly important for predicting future scenarios related to water availability.

The harmonic and isotopic analyses conducted in this study have proven to be essential tools for understanding the recharge dynamics of the Promise Spring aquifer system. The hydrodynamic behavior of the spring revealed a clear correlation between environmental variables and their temporal variations. The main discharge peaks were associated with the completion of the snowmelt process between April and May, indicating that snowmelt was one of the primary water sources that fed the spring. Furthermore, since the 2018–2019 hydrological year, altered meteorological conditions have modified snow accumulation regimes at higher altitudes in the catchment area, resulting in an increase in discharge and the temporal shift of the recession curve minima towards the autumn and winter months. Harmonic analyses further confirmed the influence of temperature changes on the hydrological behavior of the spring. Specifically, the long-term time series analysis revealed a decline in snow depth associated with an increase in atmospheric temperature. These conditions have reduced snow accumulation in the recharge area of Promise Spring, leading to an increased supply of liquid water that feeds the fractured network of the Promise aquifer during the autumn and winter months. In future research, the analysis of datasets to accurately investigate the decade response of this site under climate change effects would be a valuable perspective.

Isotopic analyses helped determine the origin of the feeding waters at the Promise Spring and Rutor Falls sampling points. The results revealed that Rutor Falls is directly fed by glacial meltwater, whereas the Promise Spring sample exhibited isotopic contents that indicate the absence of glacial contributions and instead imply a more meteoric origin, derived from snowmelt and precipitation.

The methodological approach employed in this study, which integrates harmonic and isotopic analyses, has been shown to be a useful tool for understanding spring behavior. This approach allows for a more complete and detailed view of the aquifer system, which is essential for the sustainable management of water resources, especially in settings where natural resources are sensitive to climate change. If applied to springs used for drinking water, this methodology could have significant social implications. Indeed, knowing the precise origin and nature of spring water and the recharge dynamics of the spring system allows for the improved management of water resources.

Author contribution Martina Gizzi: Conceptualization, Funding acquisition, Methodology, Investigation, Validation, Supervision, Writing – original draft, Writing – review and editing. Luca Biamino: Investigation, Methodology, Data Curation, Formal analysis, Validation, Writing – original draft, Writing – review and editing.

Funding This research was carried out as part of the "ISO4SPRINGS – Isotope investigations for identifying the water sources and recharge areas of mountain springs in the Aosta Valley Region" project. This initiative was funded in memory of Roberto Revelli and coordinated by young researchers from the Department of Environment, Land, and Infrastructure Engineering (Politecnico di Torino). Link to the project website: https://www.diati.polito.it/focus/finanziamento_di_progetti_di_ricerca_in_memoria_di_roberto_revelli

Data availability Data acquired in this study are available on request by contacting the corresponding author.

Declarations

Competing interests The authors declare that they have no competing interests.

References

Balugani E, Antonellini M (2011) Barometric pressure influence on water table fluctuations in coastal aquifers of partially enclosed seas: An example from the Adriatic coast Italy. J Hydrol 400(1):176–186. https://doi.org/10.1016/j.jhydrol.2011.01.040

Bortolami GC, Ricci B, Susella GF, Zuppi GM (1979) Isotope hydrology of the Val Corsaglia, Maritime Alps, Piedmont, Italy. International Atomic Energy Agency (IAEA): IAEA. Available at: http://inis.iaea.org/search/search.aspx?orig_q=RN:10460879.

Brigham EO, Morrow RE (1967) The fast Fourier transform. IEEE Spectr 4(12):63–70. https://doi.org/10.1109/MSPEC.1967.5217220

Cabina di Regia dei Ghiacciai Valdostani (2022) 'sottoZero 2022, Evoluzione della Criosfera in Valle d'Aosta'. Fondazione Montagna Sicura. Available at: https://www.fondazionemontagnasicura.org/sottozero.

Carroll RWH, Deems JS, Niswonger R, Schumer R, Williams KH (2019) The importance of interflow to groundwater recharge in a snowmelt-dominated headwater basin. Geophys Res Lett 46(11):5899–5908. https://doi.org/10.1029/2019GL082447

Cerino Abdin E (2021) Reliability of spring recession curve analysis as a function of the temporal resolution of the monitoring dataset. Environ Earth Sci 80(7):1–12. https://doi.org/10.1007/s12665-021-09529-2

Chizhova J, Kireeva M, Rets E, Ekaykin A, Kozachek A, Veres A, Zolina O, Varentsova N, Gorbarenko A, Povalyaev N, Plotnikova V, Samsonov T, Kharlamov M (2022) Stable isotope (δ18O, δ2H) signature of river runoff, groundwater, and precipitation in three river basins in the center of East European Plain. Earth Syst Sci Data Discuss 2022:1–14. https://doi.org/10.5194/essd-2022-377

Colucci RR, Guglielmin M (2019) Climate change and rapid ice melt: Suggestions from abrupt permafrost degradation and ice melting in an alpine ice cave. Prog Phys Geography: Earth Environ 43(4):561–573. https://doi.org/10.1177/0309133319846056

Corte E, Ajmar A, Camporeale C, Cina A, Coviello V, Giulio Tonolo F, Godio A, Macelloni MM, Tamea S, Vergnano A (2024) Multitemporal characterization of a proglacial system: a multidisciplinary approach. Earth Syst Sci Data 16(7):3283–3306. https://doi.org/10.5194/essd-16-3283-2024

Craig H (1961a) Isotopic variations in meteoric waters. Science 133(3465):1702–1703. https://doi.org/10.1126/science.133.3465.1702

Craig H (1961b) Standard for reporting concentrations of deuterium and oxygen-18 in natural waters. Science 133(3467):1833–1834. https://doi.org/10.1126/science.133.3467.1833

Crepaldi S, De Maio M, Suozzi E (2015) Preliminary Study on the Snow-Melt for the Groundwater Recharge Estimated by an Advanced Meteorological Station, in A. and C.J. and S.W. and C.M. Lollino Giorgio and Manconi (ed.) Engineering Geology for Society and Territory - Volume 1. Cham: Springer International Publishing, pp. 109–112.

Dansgaard W (1964) Stable isotopes in precipitation. Tellus 16(4):436–468. https://doi.org/10.3402/tellusa.v16i4.8993

de Palézieux L, Loew S (2019) Long-term transient groundwater pressure and deep infiltration in Alpine mountain slopes (Poschiavo Valley, Switzerland). Hydrogeol J 27(8):2817–2834. https://doi.org/10.1007/s10040-019-02025-9

DeWalle DR, Rango A (2008) Principles of Snow Hydrology. Cambridge University Press, Cambridge. https://doi.org/10.1017/CBO9780511535673

Dey S, Bhatt D, Haq S, Mall RK (2020) Potential impact of rainfall variability on groundwater resources: a case study in Uttar Pradesh, India. Arabian J Geosci 13. https://doi.org/10.1007/s12517-020-5083-8.

Donnelly C, Greuell W, Andersson J, Gerten D, Pisacane G, Roudier P, Ludwig F (2017) Impacts of climate change on European hydrology at 1.5, 2 and 3 degrees mean global warming above preindustrial level. Clim Change 143:13–26. https://doi.org/10.1007/s10584-017-1971-7

Duratorre T, Bombelli GM, Menduni G, Bocchiola D (2020) Hydropower potential in the Alps under climate change scenarios. The Chavonne Plant, Val D'Aosta. Water 12(7). https://doi.org/10.3390/w12072011.

Gat JR (1971) Comments on the stable isotope method in regional groundwater investigations. Water Resour Res 7(4):980–993. https://doi.org/10.1029/WR007i004p00980

Giustini F, Brilli M, Patera A (2016) Mapping oxygen stable isotopes of precipitation in Italy. J Hydro: Region Stud 8:162–181. https://doi.org/10.1016/j.ejrh.2016.04.001

Gizzi M, Mondani M, Taddia G, Suozzi E, Lo Russo S (2022) Aosta Valley Mountain Springs: a preliminary analysis for understanding variations in water resource availability under climate change. Water 14(7). https://doi.org/10.3390/w14071004.

Gizzi M, Narcisi R, Mondani M, Taddia G (2023) Comprehending mountain springs' hydrogeological perspectives under climate change in Aosta Valley (northwestern Italy): new automated tools and simplified approaches. Italian J Eng Geol Environ (Special Issue 1):73–80. https://doi.org/10.4408/IJEGE.2023-01.S-10

Jódar J, González-Ramón A, Martos-Rosillo S, Heredia J, Herrera C, Urrutia J, Caballero Y, Zabaleta A, Antigüedad I, Custodio E, Lambán LJ (2020) Snowmelt as a determinant factor in the hydrogeological behaviour of high mountain karst aquifers: The Garcés karst system, Central Pyrenees (Spain). Sci Total Environ 748:141363. https://doi.org/10.1016/J.SCITOTENV.2020.141363

Kim H, Villarini G (2023) On the attribution of annual maximum discharge across the conterminous United States. Adv Water Resour 171:104360. https://doi.org/10.1016/j.advwatres.2022.104360

Kresic N, Bonacci O (2010) Spring discharge hydrograph, Groundwater Hydrology of Springs, pp. 129–163. https://doi.org/10.1016/B978-1-85617-502-9.00004-9.

Leis JW (2011) Digital signal processing using MATLAB for students and researchers / John W. Leis. Wiley Blackwell, Chicester

Leontiadis IL, Payne BR, Letsios A, Papayanni N, Kakarelis D, Hadjiagorakis D (1983) Isotope hydrology study of Kato Nevrokopi, Drama Dept. Greece. Available at: http://inis.iaea.org/search/search.aspx?orig_q=RN:16026637.

Lo Russo S, Amanzio G, Ghione R, De Maio M (2014) Recession hydrographs and time series analysis of springs monitoring data: application on porous and shallow aquifers in mountain areas (Aosta Valley). Environmental Earth Sciences, 73. https://doi.org/10.1007/s12665-014-3916-z.

Lo Russo S, Suozzi E, Gizzi M, Taddia G (2021) SOURCE: a semi-automatic tool for spring-monitoring data analysis and aquifer characterisation. Environmental Earth Sciences, 80. https://doi.org/10.1007/s12665-021-10027-8

Longoni L, Panzeri L, Mondani M, Papini M (2022) Experimental analysis of seasonal processes in shallow landslide in a snowy region through downscaled and in situ observation, in EGU General Assembly Conference Abstracts. (EGU General Assembly Conference Abstracts), pp. EGU22–8247. https://doi.org/10.5194/egusphere-egu22-8247.

Magnusson J, Kobierska F, Huxol S, Hayashi M, Jonas T, Kirchner JW (2014) Meltwater driven stream and groundwater stage fluctuations on a glacier forefield (Dammagletscher, Switzerland). Hydrol Process 28(3):823–836. https://doi.org/10.1002/hyp.9633

Mazor E (2004) Chemical and Isotopic Groundwater Hydrology, 3rd edn. Marcel Dekker Inc., New York - Basel

Mercalli L, Cat Berro D, Montuschi S (2003) Atlante climatico della Valle d'Aosta. Torino: Societá Meteorologica Subalpina (Memorie dell'atmosfera 2).

Mo C, Ruan Y, He J, Jin JL, Liu P, Sun G (2019) Frequency analysis of precipitation extremes under climate change. Int J Climatol 39(3):1373–1387. https://doi.org/10.1002/joc.5887

Mondani M, Gizzi M, Taddia G (2022) Role of Snowpack-Hydrometeorological Sensors for Hydrogeological System Comprehension inside an Alpine Closed-Basin'. https://doi.org/10.3390/s22197130.

Neto DC, Chang HK, van Genuchten M (2016) A mathematical view of water table fluctuations in a shallow aquifer in Brazil. Groundwater 54(1):82–91. https://doi.org/10.1111/gwat.12329

Newlands NK, Mari C, Tye R, De Jong C (2015) Challenges for mountain hydrology in the third millennium. Frontiers in Environmental Science | www.frontiersin.org, 1, p. 38. https://doi.org/10.3389/fenvs.2015.00038.

Novel JP, Ravello M, Dray M, Pollicini F, Zuppi GM (1995) Isotopic contribution (18O, 2H, 3H) in the understanding of the flow pattern in surface water and groundwater in the Aosta Valley (Italy). Geogr Fis Din Quat 18:315–319

Orusa T, Mondino EB, Mcnulty S (2021) Exploring short-term climate change effects on rangelands and broad-leaved forests by

free satellite data in Aosta Valley (northwest Italy). https://doi.org/10.3390/cli9030047.
Pasquini AI, Lecomte KL, Depetris PJ (2008) Climate change and recent water level variability in Patagonian proglacial lakes Argentina. Glob Planet Change 63(4):290–298. https://doi.org/10.1016/j.gloplacha.2008.07.001
Payne BR, Yurtsever Y (1974) Environmental isotopes as a hydrogeological tool in Nicaragua. IAEA: IAEA, Vienna (Austria). Available at: Conference: Symposium on isotope techniques in groundwater hydrology, Vienna (Austria), 11–15 Mar 1974.
Rahi KA, Halihan T (2013) Identifying aquifer type in fractured rock aquifers using harmonic analysis. Groundwater 51(1):76–82. https://doi.org/10.1111/j.1745-6584.2012.00925.x
Riedel T, Weber TKD (2020) Review: The influence of global change on Europe's water cycle and groundwater recharge. Hydrogeol J 28(6):1939–1959. https://doi.org/10.1007/s10040-020-02165-3
Santillán-Quiroga LM, Cocca D, Lasagna M, Marchina C, Destefanis E, Forno MG, Gattiglio M, Vescovo G, De Luca DA (2023) Analysis of the recharge area of the Perrot Spring (Aosta Valley) using a hydrochemical and isotopic approach. Water 15(21). https://doi.org/10.3390/w15213756
Schmidt R, Petrovic S, Güntner A, Barthelmes F, Wünsch J, Kusche J (2008) Periodic components of water storage changes from GRACE and global hydrology models. J Geophys Res: Solid Earth 113(B8). https://doi.org/10.1029/2007JB005363
Solórzano-Rivas SC, Werner AD, Irvine DJ (2021) Estimating hydraulic properties from tidal propagation in circular islands. J Hydrol 598:126182. https://doi.org/10.1016/j.jhydrol.2021.126182
Stöckli R, Vidale PL (2004) European plant phenology and climate as seen in a 20-year AVHRR land-surface parameter dataset. Int J Remote Sens 25:3303–3330. https://doi.org/10.1080/01431160310001618149
Szwed M (2019) Variability of precipitation in Poland under climate change. Theoret Appl Climatol 135(3–4):1003–1015. https://doi.org/10.1007/s00704-018-2408-6
Thakur N, Rishi M, Keesari T, Sharma DA, Sinha UK (2020) Assessment of recharge source to springs in upper Beas basin of Kullu region, Himachal Pradesh, India using isotopic signatures. J Radioanal Nucl Chem 323(3):1217–1225. https://doi.org/10.1007/s10967-019-06617-3
Thibert E, Dkengne Sielenou P, Vionnet V, Eckert N, Vincent C (2018) Causes of glacier melt extremes in the Alps since 1949. Geophys Res Lett 45(2):817–825. https://doi.org/10.1002/2017GL076333
Vergnano A, Oggeri C, Godio A (2023) Geophysical–geotechnical methodology for assessing the spatial distribution of glacio-lacustrine sediments: The case history of Lake Seracchi. Earth Surf Proc Land 48(7):1374–1397. https://doi.org/10.1002/esp.5555
Wang H, Wang F, Sun J, Cheng Z, Wang Y, Cao Y (2023) New strategy for evaluating the spatiotemporal distribution of groundwater resource quantity under seasonal freeze/thaw in mountainous areas. J Hydrol 616:128850. https://doi.org/10.1016/j.jhydrol.2022.128850
Wu WY, Lo M, Wada Y, Famiglietti JS, Reager JT, Yeh PJF, Ducharne A, Yang ZL (2020) Divergent effects of climate change on future groundwater availability in key mid-latitude aquifers. Nat Commun 11(1):1–9. https://doi.org/10.1038/s41467-020-17581-y
Wu X, Che T, Li X, Wang X, Yang X (2018) Slower snowmelt in spring along with climate warming across the northern hemisphere. Geophys Res Lett 45(22):12, 312–331, 339. https://doi.org/10.1029/2018GL079511
Xanke J, Liesch T (2022) Quantification and possible causes of declining groundwater resources in the Euro-Mediterranean region from 2003 to 2020. Hydrogeol J 30(2):379–400. https://doi.org/10.1007/s10040-021-02448-3
Xanke J, Stevanović Z, Liesch T, Kaltenbrunn A, Ravbar N, Jourde H, Andreo B, Barberá JA, Goldscheider N (2024) Flooding and flood water storage in karst systems of the Mediterranean region. Hydrogeol J 32(6):1587–1605. https://doi.org/10.1007/s10040-024-02811-0
Xie C, Ding Y, Liu S, Chen C (2006) Response of meltwater runoff to air-temperature fluctuations on Keqikaer Glacier, south slope of Tuomuer Mountain, western China. Ann Glaciol 43:275–279. https://doi.org/10.3189/172756406781812294
Yu S, Chae G, Oh J, Kim S-H, Kim D-I, Yun S-T (2021) Hydrochemical and isotopic difference of spring water depending on flow type in a stratigraphically complex karst area of South Korea. Front Earth Sci 9. https://doi.org/10.3389/feart.2021.712865
Zemp M, Frey H, Gärtner-Roer I, Nussbaumer SU, Hoelzle M, Paul F et al (2015) Historically unprecedented global glacier decline in the early 21st century. J Glaciol 61(228):745–762. https://doi.org/10.3189/2015JoG15J017
Zuecco G, Carturan L, De Blasi F, Seppi R, Zanoner T, Penna D, Borga M, Carton A, Dalla Fontana G (2019) Understanding hydrological processes in glacierized catchments: Evidence and implications of highly variable isotopic and electrical conductivity data. Hydrol Process 33(5):816–832. https://doi.org/10.1002/hyp.13366